

Consist-Retinex: One-Step Noise-Emphasized Consistency Training Accelerates High-Quality Retinex Enhancement

Jian Xu

South China University of Technology

2713091379@qq.com

Shigui Li

South China University of Technology

John Paisley

Columbia University

Wei Chen

South China University of Technology

Delu Zeng

South China University of Technology

dlzeng@scut.edu.cn

Qibin Zhao

RIKEN AIP

Qibin.zhao@riken.jp

Abstract

Diffusion models have achieved remarkable success in low-light image enhancement through Retinex-based decomposition, yet their requirement for hundreds of iterative sampling steps severely limits practical deployment. While recent consistency models offer promising one-step generation for unconditional synthesis, their application to conditional enhancement remains unexplored. We present **Consist-Retinex**, the first framework adapting consistency modeling to Retinex-based low-light enhancement. Our key insight is that conditional enhancement requires fundamentally different training dynamics than unconditional generation—standard consistency training focuses on low-noise regions near the data manifold, while conditional mapping critically depends on large-noise regimes that bridge degraded inputs to enhanced outputs. We introduce two core innovations: (1) a **dual-objective consistency loss** combining temporal consistency with ground-truth alignment under randomized time sampling, providing full-spectrum supervision for stable convergence; and (2) an **adaptive noise-emphasized sampling strategy** that prioritizes training on large-noise regions essential for one-step conditional generation. On VE-LOL-L, Consist-Retinex achieves **state-of-the-art performance with single-step sampling (PSNR: 25.51 vs. 23.41, FID: 44.73 vs. 49.59 compared to Diff-Retinex++)**, while requiring only **1/8 of the training budget** relative to the 1000-step Diff-Retinex baseline.

1. Introduction

Low-light image enhancement constitutes a fundamental problem in computational photography, with applications ranging from mobile imaging to autonomous navigation. Classical Retinex theory [18] provides an elegant framework by factorizing images into reflectance and illumination components, enabling principled lighting manipulation while preserving scene structure.

Recent diffusion probabilistic models have revolutionized low-light enhancement through Retinex integration. Diff-Retinex [42] applies separate diffusion processes to illumination and reflectance maps, achieving unprecedented quality via iterative refinement. However, this success incurs prohibitive computational cost: 1000 sequential denoising steps render them impractical for real-time applications.

While accelerating diffusion models has attracted significant research [19, 23, 28, 29], existing methods face fundamental trade-offs: ODE solvers still require 10–50 steps, while distillation demands expensive teacher models. Consistency models [31] recently emerged as a breakthrough for one-step *unconditional* generation, achieving 1000× speedup by enforcing self-consistency along probability flow ODE trajectories.

However, consistency models remain unexplored for *conditional* generation tasks like low-light enhancement. Direct application to our framework encountered severe instabilities, revealing a critical mismatch: **standard consistency training employs log-uniform time schedules concentrating training near the data manifold ($\sigma \approx 0$), optimal for unconditional generation.** In conditional en-

hancement, however, *large-noise regions* ($\sigma \approx \sigma_{\max}$) are *critical*—where degraded inputs must integrate with target distributions. Standard schedules allocate minimal focus here, leaving conditional mappings undertrained. Moreover, existing consistency objectives lack supervision tailored to paired data $(x_{\text{low}}, x_{\text{high}})$ available in restoration tasks.

We present **Consist-Retinex**, the first framework adapting consistency models to conditional Retinex enhancement through reformulated training dynamics:

- (1) **Dual-Objective Consistency Loss** combines temporal consistency across conditional trajectories with ground-truth alignment under randomized time sampling, providing full-spectrum supervision for stable one-step generation.
- (2) **Adaptive Noise-Emphasized Sampling** allocates training focus to large-noise regions ($\sigma > \tau \cdot \sigma_{\max}$) critical for one-step conditional inference, departing from standard log-uniform sampling.
- (3) **Retinex-Consistent Architecture** applies separate consistency models $f_{\theta}^R, f_{\theta}^L$ to reflectance and illumination, each performing one-step enhancement conditioned on low-light input, with reconstruction via $\hat{I} = \hat{R} \odot \hat{L}$.

Our contributions are:

- We identify and address the fundamental mismatch between unconditional consistency training and conditional enhancement requirements.
- We establish the first principled framework for consistency-based conditional Retinex enhancement.
- We achieve **state-of-the-art on VE-LOL-L with 1-step inference (PSNR: 25.51 vs. 23.41, FID: 44.73 vs. 49.59 vs. Diff-Retinex++)**, requiring only **1/8 training budget** (200K vs. 800K iterations).

2. Related Work

2.1. Retinex-Based Low-Light Enhancement

Retinex theory [18] decomposes images as $I = R \odot L$ into reflectance and illumination components. Classical methods [6, 8, 15, 16] relied on hand-crafted priors with limited adaptability. Deep learning integration marked a paradigm shift: RetinexNet [37] pioneered end-to-end CNN decomposition, followed by learnable frameworks like KinD [47], KinD++ [48], and URetinex-Net [38]. Recent Transformer-based methods [2] further improved decomposition quality. However, these approaches suffer from error accumulation in two-stage pipelines and detail loss during reflectance denoising, while requiring numerous iterations for acceptable results.

2.2. Diffusion Models for Low-Light Enhancement

Denoising Diffusion Probabilistic Models (DDPM) [10] revolutionized image generation through iterative refinement. Diff-Retinex [42] pioneered their application to

low-light enhancement via separate diffusion processes on Retinex components, achieving unprecedented texture restoration. Extensions include Diff-Retinex++ [43] with mixture-of-experts adaptation, CLE Diffusion [44] for color correction, and GSAD [11] with structural awareness. Despite superior quality, **all diffusion-based methods require hundreds to thousands of steps** (typically 1000), rendering them impractical for real-time deployment.

2.3. Consistency Models

Song et al. [31] introduced consistency models for one-step generation by enforcing self-consistency along probability flow ODE trajectories. Through consistency distillation or training from scratch, they achieve 500–1000× speedup over DDPMs on unconditional synthesis (CIFAR-10, ImageNet). However, **consistency models remain unexplored for conditional generation**. Their log-uniform time schedule concentrates training near $\sigma \approx 0$, optimal for unconditional synthesis but mismatched for conditional tasks where large-noise regions ($\sigma \approx \sigma_{\max}$) critically bridge degraded inputs to enhanced outputs. Moreover, existing objectives lack ground-truth alignment for paired data $(x_{\text{low}}, x_{\text{high}})$, motivating our adaptation.

3. Method

3.1. Problem Setup and Preliminaries

Retinex decomposition. Classical Retinex theory [18] decomposes images as $I = R \odot L$, where $I \in \mathbb{R}^{H \times W \times 3}$ is the observed image, $R \in \mathbb{R}^{H \times W \times 3}$ denotes reflectance (intrinsic scene properties), $L \in \mathbb{R}^{H \times W \times 1}$ denotes illumination (lighting conditions), and \odot is element-wise multiplication. In low-light enhancement, given degraded input I_l with decomposition (R_l, L_l) , we recover normal-light components (R_n, L_n) that reconstruct $I_n = R_n \odot L_n$.

Diffusion and consistency models. DDPMs [10] corrupt data $x_0 \sim p_{\text{data}}$ via forward diffusion: $q(x_t | x_0) = \mathcal{N}(x_t; \sqrt{\bar{\alpha}_t}x_0, (1 - \bar{\alpha}_t)\mathbf{I})$, where $\bar{\alpha}_t = \prod_{s=1}^t (1 - \beta_s)$. Following EDM [17], we use continuous noise scale $\sigma \in [0.002, 80]$ with $\sigma^2 = (1 - \bar{\alpha})/\bar{\alpha}$. The probability flow ODE [30] provides deterministic sampling:

$$\frac{dx_t}{dt} = -\sigma(t) \frac{d\sigma(t)}{dt} \nabla_{x_t} \log p_t(x_t). \quad (1)$$

Consistency models [31] enable one-step generation via self-consistency: $f(x_t, t) = f(x_{t'}, t')$ for all $t, t' \in [\epsilon, T]$ on the same trajectory, as illustrated in Fig. 1. We adopt EDM preconditioning:

$$f_{\theta}(x, t) = c_{\text{skip}}(t) x + c_{\text{out}}(t) F_{\theta}(x, t), \quad (2)$$

where $c_{\text{skip}}(t) = \sigma_{\text{data}}^2 / [(t - \epsilon)^2 + \sigma_{\text{data}}^2]$ and $c_{\text{out}}(t) = \sigma_{\text{data}}(t - \epsilon) / \sqrt{\sigma_{\text{data}}^2 + t^2}$ with $\sigma_{\text{data}} = 0.5$.

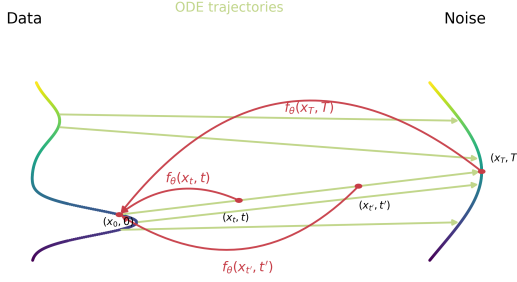


Figure 1. Illustration of consistency mapping. Green ODE trajectories evolve data samples into noise, while red arrows $f_\theta(x_t, t)$ map intermediate states back to their origin (x_ϵ, ϵ) , ensuring self-consistency along each trajectory.

3.2. Conditional Consistency for Retinex Enhancement

Framework overview. Figure 2 illustrates our Consist-Retinex framework. Given low-light image I_l and its Retinex decomposition (R_l, L_l) from TDN [42], we learn two conditional consistency models:

$$\hat{R}_n = f_\theta^R(R_n + \sigma\epsilon_R, \sigma \mid I_l), \quad (3)$$

$$\hat{L}_n = f_\theta^L(L_n + \sigma\epsilon_L, \sigma \mid I_l), \quad (4)$$

where $\epsilon_R, \epsilon_L \sim \mathcal{N}(0, \mathbf{I})$. The enhanced output is $\hat{I}_n = \hat{R}_n \odot \hat{L}_n$. At inference, we perform one-step generation from maximum noise: $\hat{R}_n = f_\theta^R(\sigma_{\max}\epsilon_R, \sigma_{\max} \mid I_l)$ (similarly for \hat{L}_n), without iterative denoising.

Training dynamics mismatch. Standard consistency training [31] uses log-uniform sampling $\sigma \sim \log \mathcal{U}(\sigma_{\min}, \sigma_{\max})$, concentrating $\sim 95\%$ of training near the data manifold ($\sigma \approx \sigma_{\min}$)—ideal for learning full data distributions from noise. However, our one-step conditional inference operates at $\sigma = \sigma_{\max}$, where the conditional signal I_l must integrate with target distributions (R_n, L_n) . Standard sampling allocates only $\sim 0.5\%$ of batches to this critical regime. Moreover, existing objectives lack explicit ground-truth alignment for paired supervision (I_l, I_n) .

3.3. Noise-Emphasized Adaptive Sampling

We rebalance training toward high-noise regions via bi-modal sampling (Fig. 3):

$$\sigma \sim \begin{cases} \log \mathcal{U}(0.95\sigma_{\max}, \sigma_{\max}), & \text{w.p. } 0.95, \\ \log \mathcal{U}(\sigma_{\min}, \sigma_{\max}), & \text{w.p. } 0.05. \end{cases} \quad (5)$$

This allocates most training to $\sigma \in [76, 80]$ where one-step inference operates, while retaining sparse full-spectrum

coverage for generalization. Empirically, low-noise loss converges rapidly (few thousand iterations), while high-noise mapping remains challenging without targeted emphasis.

3.4. Dual-Objective Consistency Loss

We combine two complementary terms with different sampling strategies: temporal consistency for trajectory coherence (standard sampling) and ground-truth alignment for conditional mapping (noise-emphasized sampling).

Temporal consistency. Following [31], we enforce self-consistency across adjacent time steps. Sample $\sigma_n, \sigma_{n+k} \sim \log \mathcal{U}(\sigma_{\min}, \sigma_{\max})$ with gap $k \sim \mathcal{U}\{1, 5\}$, construct $x_{\sigma_{n+k}} = x_0 + \sigma_{n+k}\epsilon$, and compute EMA target $\hat{x}_0^{\text{target}} = \text{sg}(f_{\theta^-}(x_{\sigma_{n+k}}, \sigma_{n+k} \mid I_l))$. Euler approximation gives:

$$x_{\sigma_n} = x_{\sigma_{n+k}} + (\sigma_n - \sigma_{n+k}) \cdot \frac{x_{\sigma_{n+k}} - \hat{x}_0^{\text{target}}}{\sigma_{n+k}}. \quad (6)$$

The loss is:

$$\mathcal{L}_{\text{consist}} = \mathbb{E}_{\epsilon, n, k} \left[w(\sigma_n) \left\| f_\theta(x_{\sigma_n}, \sigma_n \mid I_l) - \text{sg}(f_\theta(x_{\sigma_{n+k}}, \sigma_{n+k} \mid I_l)) \right\|_2^2 \right], \quad (7)$$

with SNR-based weight $w(\sigma_n) = (\sigma_{\text{data}}/\sigma_n)^2 / [1 + (\sigma_{\text{data}}/\sigma_n)^2]$. Target network updates: $\theta^- \leftarrow \mu\theta^- + (1-\mu)\theta$ with $\mu(k) = \min(0.9999, (1+k)/(10+k))$.

Ground-truth alignment. We anchor predictions to enhanced components using noise-emphasized sampling:

$$\mathcal{L}_{\text{fixed}} = \mathbb{E}_{\epsilon, \sigma_{\text{rand}}} \left[\left\| f_\theta(x_0 + \sigma_{\text{rand}}\epsilon, \sigma_{\text{rand}} \mid I_l) - x_0 \right\|_2^2 \right], \quad (8)$$

where σ_{rand} follows Eq. 5. This concentrates supervision at $\sigma \approx \sigma_{\max}$ where inference occurs.

Combined objective. The final loss is:

$$\mathcal{L}_{\text{total}} = \lambda_{\text{consist}} \mathcal{L}_{\text{consist}} + \lambda_{\text{fixed}} \mathcal{L}_{\text{fixed}}, \quad (9)$$

with $\lambda_{\text{consist}} = 1.0$ and $\lambda_{\text{fixed}} = 0.3$. This dual-objective, dual-sampling design yields stable training: Consist-Retinex converges in 200K iterations (batch size 8) vs. 800K iterations (batch size 16) for diffusion baselines [42, 43].

3.5. Architecture

Input conditioning. We concatenate low-light image and scaled noisy component: $\text{Input} = [I_l, c_{\text{in}}(\sigma) \cdot (x_0 + \sigma\epsilon)]$, where $c_{\text{in}}(\sigma) = 1/\sqrt{\sigma^2 + \sigma_{\text{data}}^2}$. This yields $[B, 6, H, W]$ for reflectance and $[B, 4, H, W]$ for illumination.

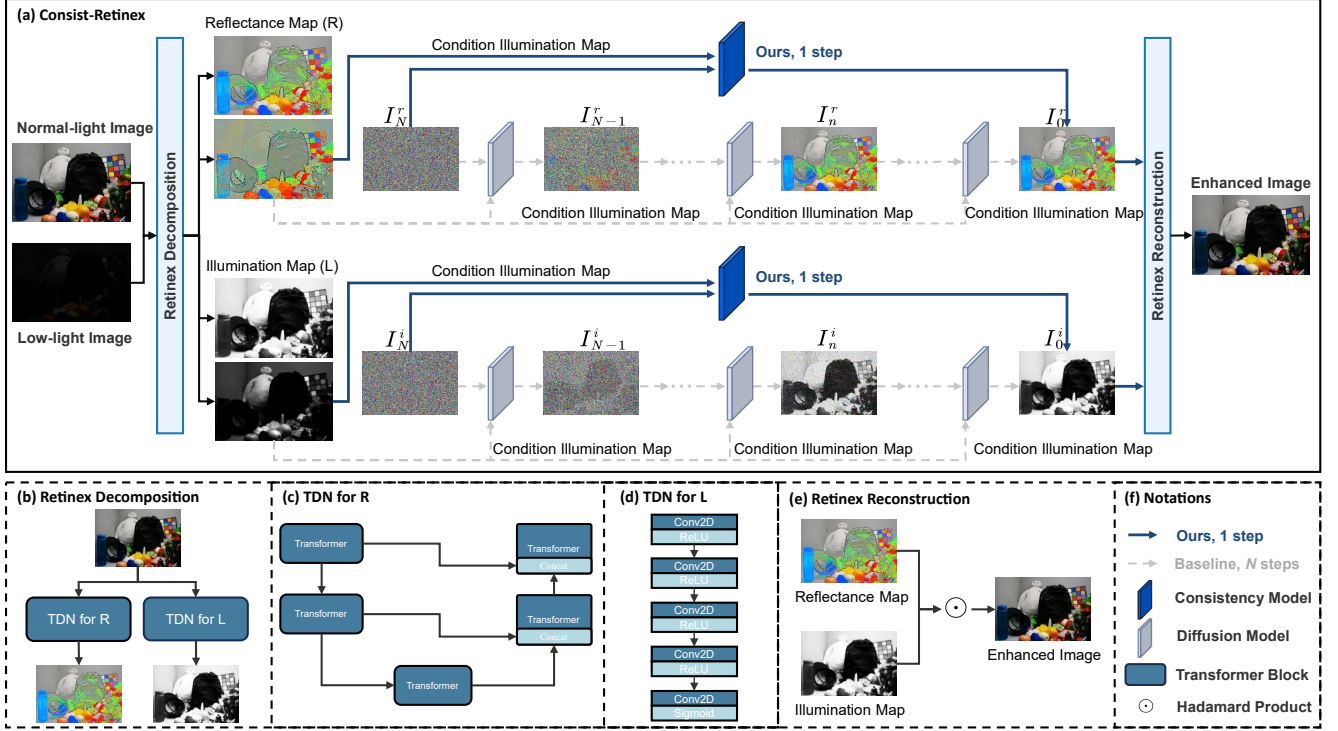


Figure 2. Overview of Consist-Retinex framework. Given a low-light image I_L , we first perform Retinex decomposition to obtain (R_L, L_L) . Two conditional consistency models f_θ^R and f_θ^L directly map noisy components to enhanced outputs in one step, guided by the low-light input. The final result is reconstructed via element-wise multiplication.

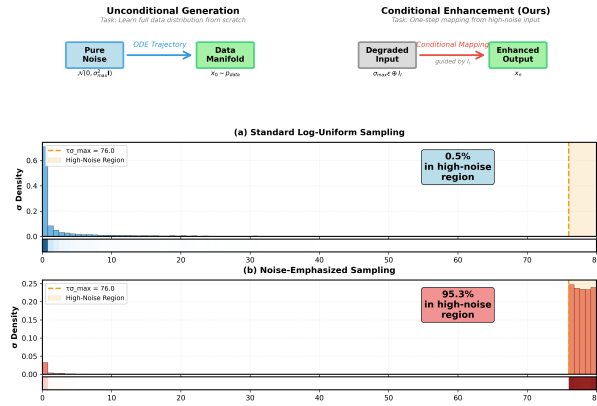


Figure 3. **Task-driven sampling strategy comparison.** *Top:* Task formulations differ fundamentally—unconditional generation learns the full data distribution from pure noise, while our conditional enhancement performs one-step mapping from *concatenated inputs* of pure noise ($\sigma_{\max}\epsilon$) and degraded image (I_L). *Middle:* Standard log-uniform sampling concentrates on the data manifold, optimal for unconditional synthesis where final denoising occurs. *Bottom:* Our noise-emphasized sampling concentrates on high-noise regions where one-step conditional inference operates.

Time embedding. We embed σ via sinusoidal Fourier features (256 bands) followed by MLP, injected through Adaptive Group Normalization [4]:

$$\text{GN}(h) (1 + \gamma(t_{\text{emb}})) + \beta(t_{\text{emb}}), \quad (10)$$

where $\gamma(\cdot)$ and $\beta(\cdot)$ are learned affine transforms.

Model configurations. The reflectance consistency model f_θ^R adopts a hybrid architecture combining Restormer [45] and U-Net components, which has demonstrated superior performance for reflectance restoration in Diff-Retinex [42]. The Restormer backbone employs multi-Dconv head transposed attention (MDTA) blocks and gated-Dconv feed-forward networks (GDFN) that efficiently capture long-range dependencies for texture detail preservation, while the U-Net structure provides hierarchical feature extraction. The model configuration uses base channel width 64, channel multipliers $\{1, 2, 4, 6\}$, with 1-1-2 TransformerBlocks across three encoder levels, 2 bottleneck blocks at the deepest level, and 2 refinement blocks ($\sim 45\text{M}$ parameters). The illumination model f_θ^L uses a compact U-Net with base width 32, multipliers $\{1, 2, 2, 4\}$, and attention at resolution 16 ($\sim 12\text{M}$ parameters).



Figure 4. Qualitative comparison with the state-of-the-art low-light image enhancement methods on the LOL dataset.

Table 1. Quantitative comparison on LOL and VE-LOL-L datasets. Bold indicates the best performance.

| Methods | LOL Dataset | | | | | VE-LOL-L Dataset | | | | |
|---|-----------------|-----------------|--------------------|------------------|------------------|------------------|-----------------|--------------------|------------------|------------------|
| | PSNR \uparrow | SSIM \uparrow | LPIPS \downarrow | FID \downarrow | MAE \downarrow | PSNR \uparrow | SSIM \uparrow | LPIPS \downarrow | FID \downarrow | MAE \downarrow |
| NPE [33] | 16.97 | 0.484 | 0.400 | 118.421 | 0.142 | 17.333 | 0.464 | 0.396 | 101.875 | 0.147 |
| LIME [8] | 16.554 | 0.429 | 0.405 | 114.003 | 0.123 | 15.105 | 0.402 | 0.426 | 98.905 | 0.145 |
| RUAS [21] | 16.405 | 0.500 | 0.270 | 112.354 | 0.153 | 15.326 | 0.488 | 0.310 | 100.078 | 0.162 |
| SCI [24] | 14.784 | 0.525 | 0.333 | 110.285 | 0.135 | 17.304 | 0.540 | 0.307 | 99.231 | 0.151 |
| Zero-DCE [7] | 19.524 | 0.703 | 0.330 | 106.629 | 0.106 | 18.059 | 0.574 | 0.313 | 91.939 | 0.131 |
| SGZ [50] | 14.546 | 0.436 | 0.353 | 115.904 | 0.143 | 16.992 | 0.359 | 0.338 | 100.875 | 0.146 |
| KinD [47] | 17.648 | 0.775 | 0.175 | 78.586 | 0.123 | 20.588 | 0.818 | 0.143 | 98.949 | 0.129 |
| KinD++ [48] | 17.752 | 0.758 | 0.198 | 80.625 | 0.124 | 17.660 | 0.761 | 0.218 | 99.504 | 0.136 |
| RetinexNet [37] | 17.558 | 0.651 | 0.379 | 150.500 | 0.117 | 16.097 | 0.401 | 0.543 | 158.988 | 0.131 |
| DRBN [41] | 16.777 | 0.730 | 0.345 | 125.238 | 0.126 | 18.466 | 0.768 | 0.352 | 110.984 | 0.138 |
| DLN [32] | 21.946 | 0.807 | 0.148 | 85.729 | 0.083 | 17.878 | 0.693 | 0.300 | 95.625 | 0.121 |
| URetinex-Net [38] | 21.328 | 0.835 | - | 59.000 | 0.083 | - | - | - | 48.360 | - |
| EnlightenGAN [14] | 17.606 | 0.653 | 0.372 | 105.590 | 0.135 | 18.676 | 0.678 | 0.364 | 92.562 | 0.108 |
| GDP [5] | 15.821 | 0.541 | 0.338 | 120.478 | 0.147 | 14.412 | 0.497 | 0.363 | 100.215 | 0.142 |
| Restormer [45] | 22.156 | 0.817 | 0.151 | 72.153 | 0.078 | 21.236 | 0.820 | 0.191 | 70.714 | 0.085 |
| LLFormer [34] | 23.649 | 0.819 | 0.169 | 76.960 | 0.063 | 20.154 | 0.809 | 0.207 | 70.165 | 0.105 |
| Retinexformer [2] | 23.386 | 0.833 | 0.140 | 70.287 | 0.067 | 22.254 | 0.831 | 0.184 | 65.031 | 0.074 |
| NeRCo [40] | 22.946 | 0.786 | 0.146 | 80.742 | 0.069 | 18.490 | 0.633 | 0.414 | 200.438 | 0.111 |
| CUE [49] | 21.670 | 0.775 | 0.224 | 93.861 | 0.079 | 18.053 | 0.753 | 0.347 | 108.284 | 0.129 |
| C-Retinex [39] | 19.866 | 0.807 | 0.196 | 90.185 | 0.096 | 18.265 | 0.789 | 0.285 | 106.526 | 0.122 |
| CLE Diffusion [44] | 21.282 | 0.794 | 0.157 | 74.540 | 0.080 | 21.995 | 0.798 | 0.191 | 79.859 | 0.074 |
| QuadPrior [35] | 18.771 | 0.781 | 0.209 | 80.185 | 0.112 | 20.471 | 0.811 | 0.198 | 69.945 | 0.085 |
| PyDiff [51] | 23.275 | 0.858 | 0.107 | 50.190 | 0.074 | 21.940 | 0.841 | 0.178 | 81.571 | 0.072 |
| EnlightenDiff [3] | 23.500 | 0.840 | 0.120 | 53.200 | 0.075 | 22.100 | 0.850 | 0.115 | 48.900 | 0.070 |
| GSAD [11] | 22.978 | 0.851 | 0.103 | 49.881 | 0.076 | 20.190 | 0.847 | 0.112 | 46.765 | 0.102 |
| Diff-Retinex [42] | 21.980 | 0.863 | 0.098 | 47.850 | 0.076 | 22.206 | 0.826 | 0.126 | 47.750 | 0.080 |
| Diff-Retinex++ [43] | 24.667 | 0.867 | 0.101 | 50.771 | 0.062 | 23.413 | 0.872 | 0.134 | 49.592 | 0.064 |
| Consist-Retinex (Ours, one-step) | 22.206 | 0.826 | 0.126 | 62.586 | 0.080 | 25.512 | 0.880 | 0.106 | 44.726 | 0.0493 |

4. Experiments

4.1. Implementation Details and Datasets

Implementation Details. We implement Consist-Retinex using PyTorch [26] and train on 3 NVIDIA RTX A6000 GPUs. Both reflectance and illumination models are trained for 200K iterations with batch size 8 (2-3 samples per GPU). We employ the AdamW optimizer [22] with learning rate 10^{-4} , $\beta_1 = 0.9$, and $\beta_2 = 0.999$. Training patches are 160×160 with horizontal flipping augmentation (probability 0.5). The noise scale range is $\sigma_{\min} = 0.002$ and

$\sigma_{\max} = 80$, with $N = 10$ discrete noise levels. For noise-emphasized sampling, we set $\tau = 0.95$ and $p_{\text{large}} = 0.95$. Loss weights are $\lambda_{\text{consist}} = 1.0$ and $\lambda_{\text{fixed}} = 0.3$. The EMA decay follows $\mu(k) = \min(0.9999, \frac{1+k}{10+k})$.

Datasets. We conduct experiments on the following datasets:

- **LOL [37]:** 485 paired training images and 15 test images at 600×400 resolution.
- **VE-LOL-L [20]:** 689 paired training images and 100 test images, featuring diverse real-world scenarios.



Figure 5. Qualitative comparison with the state-of-the-art low-light image enhancement methods on the VE-LOL-L dataset.

- **VV**: 24 unpaired low-light images for zero-shot generalization evaluation.
- **DICM**: 64 unpaired low-light images for cross-dataset testing.

4.2. Comparison with State-of-the-Art Methods

We compare Consist-Retinex against representative methods from multiple categories: traditional approaches (LIME [8], JED [27]), Retinex-based methods (RetinexNet [37], KinD [47], KinD++ [48], URetinex [38], C-Retinex [39]), Transformer-based methods (Restormer [45], LLFormer [34], Retinexformer [2]), diffusion-based approaches (Diff-Retinex (1000 steps) [42], Diff-Retinex++ (1000 steps) [43], CLE Diffusion [44], PyDiff [51], GSAD [11]), and other enhancement techniques (Zero-DCE [7], EnlightenGAN [14]).

4.2.1. Quantitative Results on LOL and VE-LOL-L

Full-reference metrics. We employ PSNR, SSIM [36], LPIPS [46], FID [9], and MAE for evaluation. Table 1 presents the quantitative comparison.

On the **VE-LOL-L** dataset, Consist-Retinex achieves state-of-the-art performance with single-step inference: 25.51 dB PSNR (outperforming Diff-Retinex++ by 2.10 dB), best SSIM of 0.880, lowest LPIPS of 0.106, FID of 44.73 (4.87 reduction from Diff-Retinex++), and lowest MAE of 0.0493. These results establish new state-of-the-art across all metrics while requiring only one-step inference.

On the **LOL** dataset, Consist-Retinex demonstrates competitive performance with PSNR of 22.21 dB and SSIM of 0.826. While Diff-Retinex++ achieves higher PSNR of 24.67 dB with 1000 steps, our method excels in perceptual metrics (LPIPS: 0.126, MAE: 0.080) and provides a superior efficiency-quality trade-off with single-step inference.

4.2.2. No-Reference Evaluation on VV and DICM

For unpaired datasets, we adopt perceptual quality metrics: Perceptual Index (PI) [1] and Natural Image Quality Evaluator (NIQE) [25]. Lower values indicate better quality.

Table 2. No-reference evaluation on DICM dataset. Lower is better.

| Method | PI↓ | NIQE↓ |
|-------------------------------|--------------|--------------|
| CLE Diffusion [44] | 3.361 | 4.505 |
| DiffLL [12] | 2.936 | 3.636 |
| GDP [5] | 3.552 | 4.358 |
| Diff-Retinex [42] | 3.394 | 4.361 |
| Diff-Retinex++ [43] | 3.203 | 3.514 |
| PyDiffusion [51] | 3.792 | 4.499 |
| LightenDiffusion [13] | 3.144 | 3.724 |
| Consist-Retinex (Ours) | 2.932 | 3.826 |

DICM dataset. Table 2 presents cross-dataset evaluation results. Consist-Retinex achieves the best PI score of 2.932, outperforming DiffLL (2.936), Diff-Retinex++ (3.203), and LightenDiffusion (3.144). For NIQE, Diff-Retinex++ achieves the best score of 3.514, while our method obtains 3.826. The strong PI performance validates our method’s robustness to domain shift and demonstrates effective cross-dataset generalization despite training exclusively on LOL.

VV dataset. Table 3 shows results on the VV dataset. DiffLL achieves the best overall performance with PI: 2.351 and NIQE: 2.869, followed by LightenDiffusion (PI: 2.558, NIQE: 2.941). Consist-Retinex obtains PI: 2.974 and NIQE: 3.650, demonstrating competitive zero-shot generalization. Combined with the superior DICM results, these findings indicate our method maintains reasonable performance across diverse unpaired datasets, though with varying degrees of effectiveness depending on dataset characteristics.

4.2.3. Qualitative Comparison

Figures 4, 5, and 6 present qualitative comparisons across paired (LOL, VE-LOL-L) and unpaired (DICM, VV)

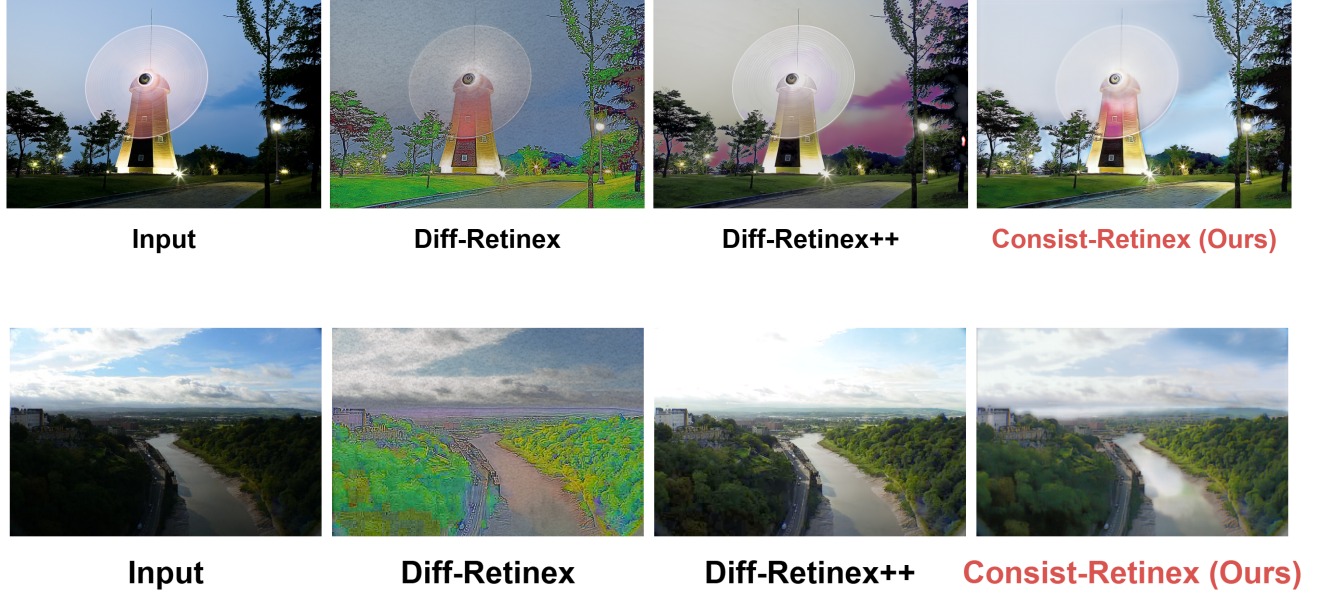


Figure 6. Qualitative comparison with the state-of-the-art low-light image enhancement methods on the DICM and VV dataset.

Table 3. No-reference evaluation on VV dataset. Lower is better.

| Method | PI↓ | NIQE↓ |
|-------------------------------|--------------|--------------|
| CLE Diffusion [44] | 3.470 | 3.240 |
| DiffLL [12] | 2.351 | 2.869 |
| GDP [5] | 3.431 | 4.683 |
| Diff-Retinex [42] | 3.350 | 3.087 |
| Diff-Retinex++ [43] | 3.643 | 3.819 |
| PyDiffusion [51] | 3.678 | 4.360 |
| LightenDiffusion [13] | 2.558 | 2.941 |
| Consist-Retinex (Ours) | 2.974 | 3.650 |

datasets. Consist-Retinex demonstrates consistent advantages in three key aspects:

Accurate color reproduction and illumination balance.

Our method maintains superior color fidelity across diverse scenarios. In Figure 4 (LOL dataset), traditional methods (RUAS, SCI) produce darker tones, while Retinex-based approaches (KinD, KinD++) exhibit unnatural color shifts. Although Diff-Retinex++ achieves relatively better results, it still shows slight color deviations. Consist-Retinex maintains natural color tones closest to the ground truth with balanced illumination, avoiding overexposure or underexposure artifacts. This advantage extends to unpaired datasets: in Figure 6 (DICM), the lighthouse scene shows

that Diff-Retinex introduces severe color artifacts (purple distortions), while Diff-Retinex++ produces an unnatural magenta cast in the sky. Our method delivers natural, visually pleasing colors without reference guidance.

Superior texture restoration and detail recovery.

Consist-Retinex excels at recovering fine-grained details from severely degraded inputs. In Figure 5 (VE-LOL-L), floor tiles and wall textures barely visible in the low-light input are cleanly restored by our method. Traditional methods (RUAS, SCI, Zero-DCE) produce over-smoothed results losing texture details, while some approaches (KinD, SGZ) introduce bluish or greenish color distortions. In the VV dataset (Figure 6, aerial river scene), Diff-Retinex generates noticeable artifacts with color distortions in vegetation and water regions, whereas Diff-Retinex++ over-brightens the water surface, losing natural appearance. Our one-step generation preserves natural textures and realistic scene details across both paired and unpaired test cases.

Effective noise suppression with preserved sharpness.

Our noise-emphasized training strategy enables robust denoising while preserving sharp details. Traditional methods (RUAS, Zero-DCE, SGZ) retain visible noise in flat regions or introduce color artifacts, while some diffusion approaches (Diff-Retinex) produce over-smoothed outputs lacking fine details. Consist-Retinex delivers clean, artifact-free enhancement with minimal noise amplification, as ev-

Table 4. Ablation study on LOL and VE-LOL-L datasets. GT: ground-truth alignment loss; NE: noise-emphasized sampling.

| GT | NE | LOL Dataset | | | VE-LOL-L Dataset | | |
|--------------|--------------|-----------------|-----------------|--------------------|------------------|-----------------|--------------------|
| | | PSNR \uparrow | SSIM \uparrow | LPIPS \downarrow | PSNR \uparrow | SSIM \uparrow | LPIPS \downarrow |
| \times | \times | 9.34 | 0.485 | 0.385 | 10.51 | 0.528 | 0.362 |
| \checkmark | \times | 18.82 | 0.752 | 0.189 | 20.05 | 0.821 | 0.165 |
| \checkmark | \checkmark | 22.21 | 0.826 | 0.126 | 25.51 | 0.880 | 0.106 |

identified in both the DICM lighthouse (smooth sky gradients without banding) and VV aerial scenes (clean foliage and water surfaces). This demonstrates that our method achieves visually pleasing results rivaling 1000-step diffusion methods with only single-step inference, generalizing effectively to unseen data distributions.

4.3. Ablation Study

We conduct ablation experiments on LOL and VE-LOL-L datasets to validate the effectiveness of our core components: ground-truth alignment loss and noise-emphasized sampling.

Experimental setup. We train three variants with identical settings except the studied components:

- **Baseline:** Standard consistency training [31] with log-uniform sampling and only temporal consistency loss $\mathcal{L}_{\text{consist}}$.
- **+ GT Alignment:** Baseline with added fixed-point alignment loss $\mathcal{L}_{\text{fixed}}$ using standard log-uniform sampling.
- **Consist-Retinex (Full):** Complete framework with dual-objective loss and noise-emphasized sampling.

Results and analysis. Table 4 demonstrates the effectiveness of each component across both datasets.

Ground-truth alignment loss ($\mathcal{L}_{\text{fixed}}$) provides substantial improvements on both datasets: +9.48 dB PSNR on LOL and +9.54 dB on VE-LOL-L. This validates our key insight that conditional enhancement requires explicit anchoring to ground-truth targets beyond temporal consistency. Unlike unconditional generation where $\mathcal{L}_{\text{consist}}$ alone suffices, conditional mapping critically depends on direct supervision at the inference noise level ($\sigma = \sigma_{\text{max}}$), where the model must bridge degraded inputs to enhanced outputs in a single step.

Noise-emphasized sampling provides additional gains when combined with GT alignment: +3.39 dB PSNR on LOL and +5.46 dB on VE-LOL-L. Standard log-uniform sampling allocates $\sim 95\%$ of training iterations near the data manifold ($\sigma \approx 0$), leaving the critical high-noise regime ($\sigma \approx \sigma_{\text{max}}$) undertrained. Our bimodal strategy (Eq. 5) concentrates 95% of $\mathcal{L}_{\text{fixed}}$ training on $\sigma > 0.95\sigma_{\text{max}}$, directly targeting where one-step inference operates. The larger improvement on VE-LOL-L suggests noise-emphasized sampling is particularly beneficial for complex, diverse scenes.

Table 5. Training efficiency comparison.

| Method | Iterations | Batch Size | Total Budget |
|-------------------------------|-------------|------------|--------------|
| Diff-Retinex [42] | 800K | 16 | 12.8M |
| Diff-Retinex++ [43] | 800K | 16 | 12.8M |
| Consist-Retinex (Ours) | 200K | 8 | 1.6M |

Synergistic effect: The full model achieves **22.21 dB** on LOL and **25.51 dB** on VE-LOL-L, demonstrating the complementary nature of our dual-objective, dual-sampling design. $\mathcal{L}_{\text{consist}}$ with standard sampling maintains theoretical consistency across all noise levels, while $\mathcal{L}_{\text{fixed}}$ with noise-emphasized sampling provides targeted supervision where inference operates, enabling both stable and efficient training.

4.4. Efficiency Analysis

Inference efficiency. Consist-Retinex achieves true one-step inference for both Retinex components:

- Reflectance model f_{θ}^R : 0.0425 s/image (26.21 dB on VE-LOL-L)
- Illumination model f_{θ}^L : 0.0357 s/image (27.22 dB on VE-LOL-L)
- Total pipeline: ~ 0.08 s/image

For 400×600 images on dual RTX A6000 GPUs, the inference throughput reaches ~ 27 FPS, enabling real-time deployment on standard hardware. This corresponds to a **1000 \times speedup** over Diff-Retinex, which requires 1000 sampling steps.

Training efficiency. Table 5 compares training budgets. Consist-Retinex requires only **1/8 of the total training budget** (1.6M vs. 12.8M effective samples) while achieving superior performance, demonstrating the efficiency of consistency-based learning.

5. Discussion and Conclusion

LOL vs. VE-LOL-L performance. The higher PSNR on VE-LOL-L (25.51 dB) compared to LOL (22.21 dB) stems from inherent dataset characteristics rather than model bias: (1) *Higher image quality*—VE-LOL-L consists of real-captured images with better overall quality and less severe degradation than LOL’s mixture of synthetic and heavily degraded samples [20]; (2) *Larger test set*—VE-LOL-L’s 100 test images vs. LOL’s 15 provide more statistically reliable metrics, reducing variance from outlier cases.

Summary. We presented Consist-Retinex, the first framework successfully adapting consistency models to Retinex-based low-light enhancement. By introducing dual-objective consistency loss and noise-emphasized sampling, we address the fundamental mismatch between unconditional consistency training and conditional enhancement

requirements. Extensive experiments demonstrate that Consist-Retinex achieves state-of-the-art performance on VE-LOL-L with single-step inference (PSNR: 25.51 dB, FID: 44.73), while requiring only 1/8 of the training budget and delivering 1000 \times speedup over diffusion baselines. Future work may explore extending this framework to other conditional image restoration tasks, investigating multi-step refinement strategies, and developing task-adaptive sampling schedules for various degradation patterns.

References

- [1] Yochai Blau and Tomer Michaeli. The perception-distortion tradeoff. In *Proceedings of the IEEE conference on computer vision and pattern recognition*, pages 6228–6237, 2018. 6
- [2] Yuanhao Cai, Hao Bian, Jing Lin, Haoqian Wang, Radu Timofte, and Yulun Zhang. Retinexformer: One-stage retinex-based transformer for low-light image enhancement. In *Proceedings of the IEEE/CVF international conference on computer vision*, pages 12504–12513, 2023. 2, 5, 6
- [3] Cheuk-Yiu Chan, Wan-Chi Siu, Yuk-Hee Chan, and H Anthony Chan. Anlightendiff: Anchoring diffusion probabilistic model on low light image enhancement. *IEEE Transactions on Image Processing*, 2024. 5
- [4] Prafulla Dhariwal and Alexander Nichol. Diffusion models beat gans on image synthesis. *Advances in neural information processing systems*, 34:8780–8794, 2021. 4
- [5] Ben Fei, Zhaoyang Lyu, Liang Pan, Junzhe Zhang, Weidong Yang, Tianyue Luo, Bo Zhang, and Bo Dai. Generative diffusion prior for unified image restoration and enhancement. In *Proceedings of the IEEE/CVF conference on computer vision and pattern recognition*, pages 9935–9946, 2023. 5, 6, 7
- [6] Xueyang Fu, Delu Zeng, Yue Huang, Xiao-Ping Zhang, and Xinghao Ding. A weighted variational model for simultaneous reflectance and illumination estimation. In *Proceedings of the IEEE conference on computer vision and pattern recognition*, pages 2782–2790, 2016. 2
- [7] Chunle Guo, Chongyi Li, Jichang Guo, Chen Change Loy, Junhui Hou, Sam Kwong, and Runmin Cong. Zero-reference deep curve estimation for low-light image enhancement. In *Proceedings of the IEEE/CVF conference on computer vision and pattern recognition*, pages 1780–1789, 2020. 5, 6
- [8] Xiaojie Guo, Yu Li, and Haibin Ling. Lime: Low-light image enhancement via illumination map estimation. *IEEE Transactions on image processing*, 26(2):982–993, 2016. 2, 5, 6
- [9] Martin Heusel, Hubert Ramsauer, Thomas Unterthiner, Bernhard Nessler, and Sepp Hochreiter. Gans trained by a two time-scale update rule converge to a local nash equilibrium. *Advances in Neural Information Processing Systems*, 30, 2017. 6
- [10] Jonathan Ho, Ajay Jain, and Pieter Abbeel. Denoising diffusion probabilistic models. *Advances in Neural Information Processing Systems*, 33:6840–6851, 2020. 2
- [11] Jinhui Hou, Zhiyu Zhu, Junhui Hou, Hui Liu, Huanqiang Zeng, and Hui Yuan. Global structure-aware diffusion process for low-light image enhancement. *Advances in Neural Information Processing Systems*, 36: 79734–79747, 2023. 2, 5, 6
- [12] Hai Jiang, Ao Luo, Haoqiang Fan, Songchen Han, and Shuaicheng Liu. Low-light image enhancement with wavelet-based diffusion models. *ACM Transactions on Graphics (TOG)*, 42(6):1–14, 2023. 6, 7
- [13] Hai Jiang, Ao Luo, Xiaohong Liu, Songchen Han, and Shuaicheng Liu. Lightendiffusion: Unsupervised low-light image enhancement with latent-retinex diffusion models. In *European Conference on Computer Vision*, pages 161–179. Springer, 2024. 6, 7
- [14] Yifan Jiang, Xinyu Gong, Ding Liu, Yu Cheng, Chen Fang, Xiaohui Shen, Jianchao Yang, Pan Zhou, and Zhangyang Wang. Enlightengan: Deep light enhancement without paired supervision. *IEEE transactions on image processing*, 30:2340–2349, 2021. 5, 6
- [15] Daniel J Jobson, Zia-ur Rahman, and Glenn A Woodell. A multiscale retinex for bridging the gap between color images and the human observation of scenes. *IEEE Transactions on Image processing*, 6(7):965–976, 1997. 2
- [16] Daniel J Jobson, Zia-ur Rahman, and Glenn A Woodell. Properties and performance of a center/surround retinex. *IEEE transactions on image processing*, 6(3): 451–462, 1997. 2
- [17] Tero Karras, Miika Aittala, Timo Aila, and Samuli Laine. Elucidating the design space of diffusion-based generative models. *Advances in neural information processing systems*, 35:26565–26577, 2022. 2
- [18] Edwin H Land. The retinex theory of color vision. *Scientific american*, 237(6):108–129, 1977. 1, 2
- [19] Shigui Li, Wei Chen, and Delu Zeng. EVODiff: Entropy-aware variance optimized diffusion inference. In *The Thirty-ninth Annual Conference on Neural Information Processing Systems*, 2025. 1
- [20] Jiaying Liu, Dejia Xu, Wenhan Yang, Minhao Fan, and Haofeng Huang. Benchmarking low-light image enhancement and beyond. *International Journal of Computer Vision*, 129:1153–1184, 2021. 5, 8
- [21] Risheng Liu, Long Ma, Jiaao Zhang, Xin Fan, and Zhongxuan Luo. Retinex-inspired unrolling with cooperative prior architecture search for low-light image

- enhancement. In *Proceedings of the IEEE/CVF Conference on Computer Vision and Pattern Recognition*, pages 10561–10570, 2021. 5
- [22] Ilya Loshchilov and Frank Hutter. Decoupled weight decay regularization. *arXiv preprint arXiv:1711.05101*, 2017. 5
- [23] Cheng Lu, Yuhao Zhou, Fan Bao, Jianfei Chen, Chongxuan Li, and Jun Zhu. Dpm-solver: A fast ode solver for diffusion probabilistic model sampling in around 10 steps. *Advances in neural information processing systems*, 35:5775–5787, 2022. 1
- [24] Long Ma, Tengyu Ma, Risheng Liu, Xin Fan, and Zhongxuan Luo. Toward fast, flexible, and robust low-light image enhancement. In *Proceedings of the IEEE/CVF Conference on Computer Vision and Pattern Recognition*, pages 5637–5646, 2022. 5
- [25] Anish Mittal, Rajiv Soundararajan, and Alan C Bovik. Making a “completely blind” image quality analyzer. *IEEE Signal processing letters*, 20(3):209–212, 2012. 6
- [26] Adam Paszke, Sam Gross, Francisco Massa, Adam Lerer, James Bradbury, Gregory Chanan, Trevor Killeen, Zeming Lin, Natalia Gimelshein, Luca Antiga, et al. Pytorch: An imperative style, high-performance deep learning library. *Advances in Neural Information Processing Systems*, 32, 2019. 5
- [27] Xutong Ren, Mading Li, Wen-Huang Cheng, and Jiaying Liu. Joint enhancement and denoising method via sequential decomposition. In *2018 IEEE international symposium on circuits and systems (ISCAS)*, pages 1–5. IEEE, 2018. 6
- [28] Tim Salimans and Jonathan Ho. Progressive distillation for fast sampling of diffusion models. In *International Conference on Learning Representations*, 2022. 1
- [29] Jiaming Song, Chenlin Meng, and Stefano Ermon. Denoising diffusion implicit models. In *International Conference on Learning Representations*, 2021. 1
- [30] Yang Song, Jascha Sohl-Dickstein, Diederik P Kingma, Abhishek Kumar, Stefano Ermon, and Ben Poole. Score-based generative modeling through stochastic differential equations. In *International Conference on Learning Representations*, 2021. 2
- [31] Yang Song, Prafulla Dhariwal, Mark Chen, and Ilya Sutskever. Consistency models. In *International Conference on Machine Learning*, pages 32211–32252. PMLR, 2023. 1, 2, 3, 8
- [32] Li-Wen Wang, Zhi-Song Liu, Wan-Chi Siu, and Daniel PK Lun. Lightening network for low-light image enhancement. *IEEE Transactions on Image Processing*, 29:7984–7996, 2020. 5
- [33] Shuhang Wang, Jin Zheng, Hai-Miao Hu, and Bo Li. Naturalness preserved enhancement algorithm for non-uniform illumination images. *IEEE transactions on image processing*, 22(9):3538–3548, 2013. 5
- [34] Tao Wang, Kaihao Zhang, Tianrun Shen, Wenhan Luo, Bjorn Stenger, and Tong Lu. Ultra-high-definition low-light image enhancement: A benchmark and transformer-based method. In *Proceedings of the AAAI Conference on Artificial Intelligence*, pages 2654–2662, 2023. 5, 6
- [35] Wenjing Wang, Huan Yang, Jianlong Fu, and Jiaying Liu. Zero-reference low-light enhancement via physical quadruple priors. In *Proceedings of the IEEE/CVF conference on computer vision and pattern recognition*, pages 26057–26066, 2024. 5
- [36] Zhou Wang, Alan C Bovik, Hamid R Sheikh, and Eero P Simoncelli. Image quality assessment: from error visibility to structural similarity. *IEEE transactions on image processing*, 13(4):600–612, 2004. 6
- [37] Chen Wei, Wenjing Wang, Wenhan Yang, and Jiaying Liu. Deep retinex decomposition for low-light enhancement. *arXiv preprint arXiv:1808.04560*, 2018. 2, 5, 6
- [38] Wenhui Wu, Jian Weng, Pingping Zhang, Xu Wang, Wenhan Yang, and Jianmin Jiang. Uretinex-net: Retinex-based deep unfolding network for low-light image enhancement. In *Proceedings of the IEEE/CVF Conference on Computer Vision and Pattern Recognition*, pages 5901–5910, 2022. 2, 5, 6
- [39] Han Xu, Hao Zhang, Xunpeng Yi, and Jiayi Ma. Cretinex: A progressive color-shift aware retinex model for low-light image enhancement. *International Journal of Computer Vision*, 132(9):3610–3632, 2024. 5, 6
- [40] Shuzhou Yang, Moxuan Ding, Yanmin Wu, Zihan Li, and Jian Zhang. Implicit neural representation for cooperative low-light image enhancement. In *Proceedings of the IEEE/CVF international conference on computer vision*, pages 12918–12927, 2023. 5
- [41] Wenhan Yang, Shiqi Wang, Yuming Fang, Yue Wang, and Jiaying Liu. From fidelity to perceptual quality: A semi-supervised approach for low-light image enhancement. In *Proceedings of the IEEE/CVF conference on computer vision and pattern recognition*, pages 3063–3072, 2020. 5
- [42] Xunpeng Yi, Han Xu, Hao Zhang, Linfeng Tang, and Jiayi Ma. Diff-retinex: Rethinking low-light image enhancement with a generative diffusion model. In *Proceedings of the IEEE/CVF international conference on computer vision*, pages 12302–12311, 2023. 1, 2, 3, 4, 5, 6, 7, 8
- [43] Xunpeng Yi, Han Xu, Hao Zhang, Linfeng Tang, and Jiayi Ma. Diff-retinex++: Retinex-driven reinforced diffusion model for low-light image enhance-

- ment. *IEEE Transactions on Pattern Analysis and Machine Intelligence*, 2025. [2](#), [3](#), [5](#), [6](#), [7](#), [8](#)
- [44] Yuyang Yin, Dejie Xu, Chuangchuang Tan, Ping Liu, Yao Zhao, and Yunchao Wei. Cle diffusion: Controllable light enhancement diffusion model. In *Proceedings of the 31st ACM International Conference on Multimedia*, pages 8145–8156, 2023. [2](#), [5](#), [6](#), [7](#)
 - [45] Syed Waqas Zamir, Aditya Arora, Salman Khan, Munawar Hayat, Fahad Shahbaz Khan, and Ming-Hsuan Yang. Restormer: Efficient transformer for high-resolution image restoration. In *Proceedings of the IEEE/CVF conference on computer vision and pattern recognition*, pages 5728–5739, 2022. [4](#), [5](#), [6](#)
 - [46] Richard Zhang, Phillip Isola, Alexei A Efros, Eli Shechtman, and Oliver Wang. The unreasonable effectiveness of deep features as a perceptual metric. In *Proceedings of the IEEE Conference on Computer Vision and Pattern Recognition*, pages 586–595, 2018. [6](#)
 - [47] Yonghua Zhang, Jiawan Zhang, and Xiaojie Guo. Kindling the darkness: A practical low-light image enhancer. In *Proceedings of the ACM International Conference on Multimedia*, pages 1632–1640, 2019. [2](#), [5](#), [6](#)
 - [48] Yonghua Zhang, Xiaojie Guo, Jiayi Ma, Wei Liu, and Jiawan Zhang. Beyond brightening low-light images. *International Journal of Computer Vision*, 129:1013–1037, 2021. [2](#), [5](#), [6](#)
 - [49] Naishan Zheng, Man Zhou, Yanmeng Dong, Xiangyu Rui, Jie Huang, Chongyi Li, and Feng Zhao. Empowering low-light image enhancer through customized learnable priors. In *Proceedings of the IEEE/CVF International Conference on Computer Vision*, pages 12559–12569, 2023. [5](#)
 - [50] Shen Zheng and Gaurav Gupta. Semantic-guided zero-shot learning for low-light image/video enhancement. In *Proceedings of the IEEE/CVF Winter conference on applications of computer vision*, pages 581–590, 2022. [5](#)
 - [51] D Zhou, Z Yang, and Y Yang. Pyramid diffusion models for low-light image enhancement. In *International Joint Conference on Artificial Intelligence. IJCAI*, 2023. [5](#), [6](#), [7](#)